

Cyclotron motion and magnetic focusing in semiconductor quantum wells with spin-orbit coupling

John Schliemann

Institute for Theoretical Physics, University of Regensburg, D-93040 Regensburg, Germany

(Dated: February 2, 2008)

We investigate the ballistic motion of electrons in III-V semiconductor quantum wells with Rashba spin-orbit coupling in a perpendicular magnetic field. Taking into account the full quantum dynamics of the problem, we explore the modifications of classical cyclotron orbits due to spin-orbit interaction. As a result, for electron energies comparable with the cyclotron energy the dynamics are particularly rich and not adequately described by semiclassical approximations. Our study is complementary to previous semiclassical approaches concentrating on the regime of weaker fields.

PACS numbers: 73.21.Fg, 71.70.Ej, 73.23.Ad

I. INTRODUCTION

The coupling between the orbital and the spin degrees of freedom of itinerant carriers in semiconductors is a major direction of work in today's spintronics research. An early key example is given by the proposal of a spin field-effect transistor put forward by Datta and Das already in 1990¹. The merit of this paradigmatic theoretical concept is that it allows, once realized, all-electrical control of electron spins in two-dimensional III-V semiconductor structures, avoiding any magnetic field. On the other hand, at about the same van Houten *et al.* published a pioneering both theoretical and experimental study of magnetic focusing of electrons in semiconductor quantum wells². Here the control over the orbital degree of freedom of the carriers is achieved by a perpendicular magnetic field of typically moderate strength, very analogously to the classical cyclotron motion. This effect has been demonstrated both for conduction-band electrons² and for valence-band holes^{3,4}; very recently cyclotron orbits in an electron focusing experiment were directly imaged using scanning probe microscopy⁵.

Other recent experimental studies have addressed the question whether it is feasible to spatially separate (and, in turn, separately detect) carriers in different spin-split subbands of a quantum well via such transverse focusing techniques^{6,7,8}. In these investigations, the spin splitting of subbands was either provided by a strong in-plane component of the magnetic field⁶, or, more relevant for the present study, by specific contributions to spin-orbit coupling acting on the spin of carriers in semiconductor quantum wells^{7,8,9}. In the latter case, different initial spin states provide via spin-orbit interaction a separation of carriers in real space, an effect which has already attracted also significant theoretical interest^{10,11,12,13,14,15}. In the present paper we provide a complementary theoretical study of cyclotron motion and magnetic focusing under the influence of spin-orbit interaction using a fully quantum mechanical approach.

A related phenomenon is the predicted *zitterbewegung* of carrier wave packets in the presence of spin-orbit coupling^{16,17,18,19,20,21,22,23,24,25,26,27,28}. *Zitterbewegung*

of free electrons described by the four-component Dirac equation was originally predicted by Schrödinger and occurs for wave packets which contain solutions of the free Dirac equation of both positive and negative energy²⁹. In effective models for electrons and holes in semiconductors the intrinsic spin-dependent energy splitting due to spin-orbit coupling can lead to a similar oscillatory *zitterbewegung*^{16,17,21,25}. However, the latter effect is predicted to occur on time and length scales being much more favorable for experimental detection compared to the situation of free electrons where *zitterbewegung* has never been observed so far^{16,17}. On the other hand, a unifying aspect of these two phenomena is given by the fact that *zitterbewegung* of itinerant band carriers in semiconductors occurs due to spin-orbit interaction which can be viewed as the nonrelativistic of the strong coupling between spin and momentum being manifest in the Dirac equation.

Moreover, the interplay between spin-orbit coupling and cyclotron motion in a perpendicular magnetic field was already studied theoretically in some detail in Refs.^{25,27}. Here the authors concentrate on semiclassical approximations, and on an analogy between the Jaynes-Cummings model of atomic transitions in a radiation field and the Rashba Hamiltonian³⁰ in a perpendicular magnetic field, an aspect to be briefly reviewed below. In the present paper we report on numerical evaluations of the full quantum mechanical dynamics of a free electron in a two-dimensional quantum well with spin-orbit interaction and a perpendicular magnetic field, avoiding any further approximation. As explained in the appendix, our approach is so far technically limited to the Hilbert space of the first few ten lowest Landau levels. For typical electron energies of a few meV, this restriction corresponds for usual III-V semiconductor materials to magnetic fields of a few tesla. Such fields are somewhat larger than those considered in circumstances of semiclassical approximations neglecting Landau quantization, and in this sense our present study is complementary to those previous investigations. For definiteness we will also concentrate on spin-orbit coupling of the Rashba type, although also other effective coupling terms can be considered. Finally we note that a complementary theoretical

study of conduction-band electrons being subject to spin-orbit coupling and a homogeneous *in-plane electric field* was given very recently in Ref.²⁴.

This paper is organized as follows. In section II we summarize the essential properties of the Rashba model in a perpendicular magnetic field. We discuss the analogy to the Jaynes Cummings model of quantum optics, and we describe in detail the initial states used for the numerical simulations of time evolutions to be discussed in section III. All further technical details can be found in the appendix. We close with conclusions in section IV.

II. MODEL AND APPROACH

We consider an electron in an n-doped quantum well being subject to Rashba spin-orbit coupling³⁰ and a homogeneous perpendicular magnetic field coupling both to the orbital degrees of freedom as well as to the spin, i.e. the single-particle Hamiltonian reads

$$\mathcal{H} = \frac{\vec{\pi}^2}{2m} + \frac{\alpha}{\hbar} (\pi_x \sigma^y - \pi_y \sigma^x) + \frac{1}{2} g \mu_B B \sigma^z. \quad (1)$$

Here m the effective band mass, $\vec{\pi} = \vec{p} + e\vec{A}/c$ is the two-component kinetic momentum with the canonical momentum \vec{p} and the vector potential \vec{A} generating the magnetic field \vec{B} along the growth direction of the quantum well chosen as the z -axis, $\vec{B} = \nabla \times \vec{A}$. The effective Rashba spin-orbit coupling parameter is denoted by α , g is the effective g-factor, μ_B the Bohr magneton, and $\vec{\sigma}$ are the usual Pauli matrices. Note that the Rashba Hamiltonian can be viewed as a momentum-dependent field coupling to the electron spin, an interpretation we will use later on in the discussion of numerical results. Moreover, in the following we will assume, without loss of generality, that the product of the electron charge ($-e$) and the magnetic field strength B is always positive, $(-e)B > 0$, i.e. \vec{B} points along the negative z -direction.

A. Spectrum and eigenstates

Defining the usual bosonic operators

$$a = \frac{1}{\sqrt{2}} \frac{\ell}{\hbar} (\pi_x + i\pi_y) \quad , \quad a^\dagger = (a)^\dagger \quad (2)$$

fulfilling $[a, a^\dagger] = 1$ and $\ell = \sqrt{\hbar c / |eB|}$ being the magnetic length, the Hamiltonian reads

$$\begin{aligned} \mathcal{H} = & \hbar\omega_c \left(a^\dagger a + \frac{1}{2} \right) + \frac{i}{\sqrt{2}} \frac{\alpha}{\ell} (a\sigma^- - a^\dagger\sigma^+) \\ & + \frac{1}{2} g \mu_B B \sigma^z \end{aligned} \quad (3)$$

where $\omega_c = |eB|/(mc)$ is the cyclotron frequency, and we have defined $\sigma^\pm = \sigma^x \pm i\sigma^y$. The operators a and a^\dagger

connect different Landau levels. Note that the Hamiltonian (including the spin-orbit part) can be expressed in terms of a and a^\dagger only, no further orbital operators occur. Therefore its eigenstates have the same Landau level degeneracy as in the absence of spin-orbit coupling.

Fixing a certain intra-Landau-level quantum number, we denote by $|n, \sigma\rangle = ((a^\dagger)^n / \sqrt{n!}) |0, \sigma\rangle$ a state in the n -th Landau level with spin direction $\sigma \in \{\uparrow, \downarrow\}$. Then $|0, \uparrow\rangle$ is an eigenstate with energy $\varepsilon_0 = (\hbar\omega_c + g\mu_B B)/2$, and all other eigenstates are of the form^{30,31}

$$|n, \pm\rangle = u_n^\pm |n, \uparrow\rangle + v_n^\pm |n-1, \downarrow\rangle \quad (4)$$

with energy

$$\varepsilon_n^\pm = \hbar\omega_c n \pm \sqrt{2n \frac{m\alpha^2}{\hbar^2} \hbar\omega_c + \frac{1}{4} (\hbar\omega_c + g\mu_B B)^2} \quad (5)$$

and the amplitudes parametrizing the eigenstates read

$$u_n^\pm = \left(\frac{1}{2} \pm \frac{\frac{1}{4} (\hbar\omega_c + g\mu_B B)}{\sqrt{2n \frac{m\alpha^2}{\hbar^2} \hbar\omega_c + \frac{1}{4} (\hbar\omega_c + g\mu_B B)^2}} \right)^{\frac{1}{2}} \quad (6)$$

$$v_n^\pm = \pm i \operatorname{sgn}(\alpha) \cdot \left(\frac{1}{2} \mp \frac{\frac{1}{4} (\hbar\omega_c + g\mu_B B)}{\sqrt{2n \frac{m\alpha^2}{\hbar^2} \hbar\omega_c + \frac{1}{4} (\hbar\omega_c + g\mu_B B)^2}} \right)^{\frac{1}{2}} \quad (7)$$

Thus, the energy levels and eigenstates of the system are characterized by the interplay of three energy scales: The cyclotron energy $\varepsilon_c = \hbar\omega_c$, the Zeeman energy $\varepsilon_Z = g\mu_B B$, and the Rashba energy $\varepsilon_R = m\alpha^2/\hbar^2$.

B. Analogy to the Jaynes-Cummings model

As it was recognized recently in Ref.²⁵, the Hamiltonian (3) is formally equivalent to the Jaynes-Cummings model for atomic transitions in a radiation field. This model has been studied very intensively in theoretical quantum optics, and the time evolution of orbital and spin operators has been obtained in terms of analytical but rather implicit expressions^{32,33}. To explore this analogy it is useful to separate the Hamiltonian into two commuting parts, $\mathcal{H} = \mathcal{H}_1 + \mathcal{H}_2$, with

$$\mathcal{H}_1 = \hbar\omega_c \left(a^\dagger a + \frac{1 + \sigma^z}{2} \right), \quad (8)$$

$$\mathcal{H}_2 = \frac{i}{\sqrt{2}} \frac{\alpha}{\ell} (a\sigma^- - a^\dagger\sigma^+) - \frac{\hbar\omega_c}{2} \left(1 - \frac{gm}{2m_0} \right) \sigma^z \quad (9)$$

where m_0 is the bare electron mass. Then the time evolution of the position operators in the Heisenberg picture,

$$\vec{r}_H(t) = e^{iHt/\hbar} \vec{r}(0) e^{-iHt/\hbar}, \quad (10)$$

can be written as^{25,32,33}

$$x_H(t) + iy_H(t) = x_0 + iy_0 + \frac{ie^{-i(\omega_c + \omega_+)t}}{\omega_- - \omega_+} \left(\frac{\omega_-}{\omega_c} \frac{\pi_x + i\pi_y}{m} + i\frac{\alpha}{\hbar} \sigma^+ \right) - \frac{ie^{-i(\omega_c + \omega_-)t}}{\omega_- - \omega_+} \left(\frac{\omega_+}{\omega_c} \frac{\pi_x + i\pi_y}{m} + i\frac{\alpha}{\hbar} \sigma^+ \right), \quad (11)$$

where the operator-valued frequencies ω_{\pm} are given by

$$\hbar\omega_{\pm} = -\mathcal{H}_2 \pm \sqrt{2\frac{m\alpha^2}{\hbar^2}\hbar\omega_c + \mathcal{H}_2^2} \quad (12)$$

and x_0, y_0 are the usual coordinates of the center of the classical cyclotron orbit which commute with the Hamiltonian and are therefore constant in time.

The result (11) is correct but still not very explicit. In particular, the operator character of the quantities ω_{\pm} poses severe obstacles against evaluating this expression for a given initial state. Therefore, in the present work we follow a different route towards the full quantum dynamics by expanding the initial state of the system in terms of its eigenstates.

C. Gauge and initial state

In the very general considerations so far there was not any necessity to specify the gauge of the vector potential \vec{A} . For the practical calculations to be described below, however, we shall work in the Landau gauge $\vec{A} = (0, Bx, 0)$ where the spinless orbital eigenstates in the absence of spin-orbit coupling have the following well-known form

$$\langle \vec{r} | n, k \rangle = \frac{i^n}{\sqrt{n!2^n\ell\sqrt{\pi}}} H_n \left(\frac{x - k\ell^2}{\ell} \right) \times \exp \left(-\frac{1}{2\ell^2} (x - k\ell^2)^2 \right) \frac{e^{iky}}{\sqrt{2\pi}} \quad (13)$$

labelled by a wave number k corresponding to translational invariance in the y -direction, or, equivalently, by a guiding center coordinate $k\ell^2$ for the x -direction. $H_n(x)$ are the usual Hermite polynomials, and the phases of the above wave functions have been adjusted to fulfill $a|n, k\rangle = \sqrt{n}|n-1, k\rangle$.

In what follows we will be interested in the quantum dynamics of an initial state $|\psi\rangle$ being a direct product of an orbital and a spin state,

$$|\psi\rangle = |\phi\rangle \begin{pmatrix} \kappa \\ \lambda \end{pmatrix}, \quad (14)$$

where the spinor components are related to the usual polar angles ϑ, φ of the initial spin direction via $\kappa = \exp(-i\varphi/2)\cos(\vartheta/2)$, $\lambda = \exp(i\varphi/2)\sin(\vartheta/2)$. As a generic initial orbital state we consider

$$\langle \vec{r} | \phi \rangle = \frac{1}{\sqrt{\pi}d} e^{-\frac{r^2}{2d^2} + ik_0 y}, \quad (15)$$

i.e. a normalized Gaussian wave packet of spatial width d and initial momentum $\hbar k_0$ along the y -axis, i.e. the direction of translational invariance of the Hamiltonian. The initial position of the particle is at the origin, $\langle \psi | \vec{r} | \psi \rangle = 0$.

The energy of the above initial state can be expressed as

$$\begin{aligned} \langle \psi | \mathcal{H} | \psi \rangle &= \frac{1}{2} \hbar \omega_c \left(\frac{\ell^2}{d^2} + \frac{d^2}{2\ell^2} + k_0^2 \ell^2 \right) \\ &\quad - \sqrt{\frac{m\alpha^2}{\hbar^2}} \hbar \omega_c k_0 \ell (\bar{\kappa} \lambda + \bar{\lambda} \kappa) \\ &\quad + \frac{1}{2} g \mu_B B (\bar{\kappa} \kappa - \bar{\lambda} \lambda) \end{aligned} \quad (16)$$

where the bar denotes complex conjugation. Conversely, for a wave packet of the above form with fixed energy E and given width and spin state, the initial momentum reads

$$\begin{aligned} k_0 \ell &= \sqrt{\frac{m\alpha^2}{\hbar^2}} \frac{1}{\hbar \omega_c} (\bar{\kappa} \lambda + \bar{\lambda} \kappa) \\ &\pm \left[\frac{2E}{\hbar \omega_c} - \left(\frac{\ell^2}{d^2} + \frac{d^2}{2\ell^2} + g \mu_B B (\bar{\kappa} \kappa - \bar{\lambda} \lambda) \right) \right. \\ &\quad \left. + \frac{m\alpha^2}{\hbar^2} (\bar{\kappa} \lambda + \bar{\lambda} \kappa)^2 \right]^{1/2}. \end{aligned} \quad (17)$$

D. Time evolution

A conceptually straightforward way to evaluate time-dependent expectation values is to expand the initial state in terms of the eigenstates of the above system and use the matrix elements of the desired operator in this eigenbasis. For instance, for the kinetic-momentum operator, this approach formally reads

$$\begin{aligned} \langle \psi | \vec{\pi}_H(t) | \psi \rangle &= \sum_{n_1, n_2=0}^{\infty} \sum_{\mu_1, \mu_2} \int_{-\infty}^{\infty} dk \left[\langle \psi | n_1, k, \mu_1 \rangle \right. \\ &\quad \times \langle n_1, k, \mu_1 | \vec{\pi} | n_2, k, \mu_2 \rangle \langle n_2, k, \mu_2 | \psi \rangle \\ &\quad \left. \times \exp \left(\frac{i}{\hbar} (\varepsilon_{n_1}^{\mu_1} - \varepsilon_{n_2}^{\mu_2}) t \right) \right], \end{aligned} \quad (18)$$

where we have already anticipated that these operators are diagonal in the intra-Landau-level quantum number k ; the same holds for the spin operators $\vec{\sigma}_H(t)$. The summation over $\mu_i, i \in \{1, 2\}$ runs over $\mu_i = \pm$ for $n_i > 0$ and $\mu_i = \uparrow$ for $n_i = 0$. From the expectation values of the position operators can be obtained from those of the momenta via

$$x = x_0 + \frac{c}{eB} \pi_y, \quad (19)$$

$$y = y_0 - \frac{c}{eB} \pi_x, \quad (20)$$

where the expectation values of the constant centers of the classical cyclotron motion are given by $\langle \psi | x_0 | \psi \rangle =$

$k_0\ell^2$, $\langle\psi|y_0|\psi\rangle = 0$. As explained in detail in the appendix, the integration over the wave numbers k can be performed separately and serves as an input for the numerical evaluation of the remaining sums. For any further technical details, we refer the reader to the appendix.

III. RESULTS

We now present the results of numerical simulations of the time evolution of expectation values described in Eq. (18). All relevant technical details can be found in the appendix. In all simulation we assume the Rashba coefficient to be positive, $\alpha > 0$.

A. Cyclotron motion

Let us first investigate the influence of spin-orbit coupling on the cyclotron motion in general. Fig. 1 shows the the particle orbit evaluated in terms of the expectation values $\langle\psi|\vec{r}_H(t)|\psi\rangle =: \langle\vec{r}_H(t)\rangle$ of a wave packet of initial width $d = 1.0\ell$ and group wave number $k_0 = 2.0/\ell$ for various initial spin states. The Rashba energy is $\varepsilon_R = 0.2\hbar\omega_c$ while the Zeeman energy is, for simplicity, put to zero here. In the left (right) top panel, the spin points initially along the positive (negative) x -direction. The middle and bottom panels show the corresponding data for the y - and z -direction, respectively. The total simulation time is always $t = 30/\omega_c$. The strictly circular motion (dotted lines) with radius $k_0\ell^2$ occurring in the absence of spin-orbit coupling is shown in all graphs as a guide to the eye. The magnetic length ℓ can conveniently be converted into practical units via $\ell = 257\text{\AA}/\sqrt{B/\text{Tesla}}$.

All six graphs have the appearance of a more or less distorted spiral. The *prima vista* most regular motion is found in the two top panels where the initial spin direction is collinear with in initial direction of the momentum-dependent coupling to the spin described by the Rashba Hamiltonian. This situation was investigated very recently in Ref.²⁷ in the framework of several schemes of semiclassical approximations. In one of these approaches the spin is assumed to follow in an adiabatic fashion the momentum-dependent field coupling to it, where both quantities are taken to be classical variables. We will discuss below to what extent this approximation leads to useful results in the parameter regime considered here where the energy of the initial wave packet is comparable with the cyclotron energy.

In Fig. 2 we have plotted the corresponding spin dynamics expressed in terms of the time-dependent expectation values $\langle\vec{\sigma}_H(t)\rangle$. The initial conditions in the three panels are the same as in the left column of Fig. 1. The solid lines show the modulus of the vector $|\langle\vec{\sigma}_H(t)\rangle|$ of the time-dependent expectation values of spin components. This quantity can be used as a measure of entanglement between the electron spin and its orbital degrees of freedom^{34,35}. In fact, when tracing out the real-space

degrees of freedom, the time-dependent reduced density matrix of the spin reads

$$\begin{aligned}\rho_{spin}(t) &= \text{tr}_{orb} \left[e^{-\frac{i}{\hbar}\mathcal{H}t} |\psi\rangle\langle\psi| e^{\frac{i}{\hbar}\mathcal{H}t} \right] \\ &= \frac{1}{2} \begin{pmatrix} 1 + \langle\sigma_H^z(t)\rangle & \langle\sigma_H^+(t)\rangle \\ \langle\sigma_H^-(t)\rangle & 1 - \langle\sigma_H^z(t)\rangle \end{pmatrix} \quad (21)\end{aligned}$$

with eigenvalues $\lambda_{\pm}(t) = (1 \pm |\langle\vec{\sigma}_H(t)\rangle|)/2$. Thus, a modulus of $|\langle\vec{\sigma}_H(t)\rangle| = 1$ (as present in the initial condition at $t = 0$) corresponds to a direct product of spin and orbital state with a reduced spin density matrix of rank 1, while a vanishing modulus $|\langle\vec{\sigma}_H(t)\rangle| = 0$ indicates maximal entanglement between spin and orbital degrees of freedom, and the reduced spin density matrix is proportional to the unit matrix^{34,35}. As seen in Fig. 2, the modulus $|\langle\vec{\sigma}_H(t)\rangle|$ is generically clearly smaller than unity signalling between spin and real-space coordinates, an effect certainly beyond semiclassical approximations.

Let us now come back to the investigation of the adiabatic semiclassical approximation employed in Ref.²⁷. Here both spin and particle momentum are treated as classical variables, and the projection of the spin on the instantaneous direction of the momentum-dependent field is assumed to be constant. Intuitively, this assumption corresponds to strong spin-orbit coupling²⁷ as it is the case for a Rashba energy of $\varepsilon_R = 0.2\hbar\omega_c$ studied above. To investigate the validity of this adiabatic approximation, we introduce

$$Q_1(t) := \frac{\langle(\pi_x)_H(t)\rangle\langle\sigma_H^y(t)\rangle - \langle(\pi_y)_H(t)\rangle\langle\sigma_H^x(t)\rangle}{|\langle\vec{\pi}_H(t)\rangle|} \quad (22)$$

and

$$Q_2(t) := \frac{\langle(\pi_x)_H(t)\rangle\langle\sigma_H^y(t)\rangle - \langle(\pi_y)_H(t)\rangle\langle\sigma_H^x(t)\rangle}{|\langle\vec{\pi}_H(t)\rangle||\langle\vec{\sigma}_H(t)\rangle|} \quad (23)$$

The first quantity is the projection of the vector $\langle\vec{\sigma}_H(t)\rangle$ onto the direction of the momentum-dependent field evaluated in terms of $\langle\vec{\pi}_H(t)\rangle$, whereas in Q_2 we have additionally divided by $|\langle\vec{\sigma}_H(t)\rangle|$ in order to eliminate the effects of entanglement discussed above. For the adiabatic-semiclassical approximation to be valid, Q_1 and Q_2 should be reasonably constant in time.

Fig. 3 shows the time dependence of Q_1 and Q_2 for the same system parameters as in Fig. 1. In particular $\langle\vec{\pi}_H(0)\rangle$ points along the positive y -direction which means that the momentum-dependent field coupling to the spin is initially in the x -direction in spin space. In the top panel, the spin points initially along the positive (negative) x -direction with $Q_1(0) = Q_2(0) = +1$ ($Q_1(0) = Q_2(0) = -1$). The middle and bottom panels show the analogous data with the spin initially aligned along the y - and z -axis, respectively. Here we have always $Q_1(0) = Q_2(0) = 0$. As seen in the figure, $Q_1(t)$ and $Q_2(t)$ significantly deviate from a constant value even in the case where the spin is initially fully aligned with the momentum-dependent field (top panel). From these

observations we conclude that this adiabatic semiclassical approximation is rather problematic in the parameter regime studied here where the total energy of the electron wave packet is of the order of the cyclotron energy. In fact, the behavior of the system is only rather poorly represented by introducing two different cyclotron radii corresponding to two spin directions as suggested in Ref.²⁷. On the contrary, the dynamics are much richer and show trajectories reminiscent of chaotic behavior. The latter observation becomes even more significant at smaller initial group wave number k_0 as one can see in Fig. 4 where we have plotted trajectories analogous to those in Fig. 1 but with a shorter initial group wave vector of only $k_0 = 0.5/\ell$. For lower cyclotron energies, however, we expect the semiclassical approximation of Ref.²⁷ to be significantly better fulfilled than in the regime studied here. The smaller the cyclotron energy compared to the total energy of the wave packet, the larger the number of Landau levels to be included in the numerical simulation. As explained in the appendix, such simulations require the precise numerical evaluation of high-order Hermite polynomials, a task which technically limits our approach to the regime where the cyclotron energy is comparable with the energy of the initial wave packet. In this sense, our study is complementary to previous semiclassical approaches concentrating on the regime of weaker fields.

Finally Fig. 5 shows the orbital dynamics for again the same system as in Fig. 1 for various values of the initial group wave number k_0 and the spin initially always pointing along the positive x -axis. For a better comparison the components of $\langle \vec{r} \rangle$ are given in units of $k_0 \ell^2$. Clearly, the dynamics become more “regular” (or less “chaotic”) the larger the initial group wave number k_0 .

In the above investigations we have concentrated on the position operator $\vec{r}_H(t)$ to describe the time evolution of the initial state chosen as a Gaussian wave packet. Regarding the width of this wave packet (as opposed to its center $\langle \vec{r}_H(t) \rangle$) let us consider the case of vanishing spin-orbit coupling. Here the components of the position operator are straightforwardly obtained as

$$x_H(t) = x(0) + \frac{\pi_x(0)}{m\omega_c} \sin(\omega_c t) + \frac{\pi_y(0)}{m\omega_c} (1 - \cos(\omega_c t)), \quad (24)$$

$$y_H(t) = y(0) + \frac{\pi_y(0)}{m\omega_c} \sin(\omega_c t) - \frac{\pi_x(0)}{m\omega_c} (1 - \cos(\omega_c t)) \quad (25)$$

$$(26)$$

and are completely analogous to the classical cyclotron motion. For an initial state Gaussian wave packet given in Eq. (15) the time dependent width reads

$$\begin{aligned} & \langle x_H^2(t) \rangle - \langle x_H(t) \rangle^2 + \langle y_H^2(t) \rangle - \langle y_H(t) \rangle^2 \\ &= d^2 + \left(2 \frac{\ell^4}{d^2} - d^2 \right) (1 - \cos(\omega_c t)). \end{aligned} \quad (27)$$

Thus, differently from the dispersive dynamics of a wave packet in the absence of a magnetic field, the width does not increase to infinity but remains bounded and rather oscillates with the cyclotron frequency, similarly to the time evolution of a coherent state in a harmonic oscillator. In the presence of spin-orbit coupling we expect the time evolution of the width of the initial state to be more complex but still essentially bounded.

B. Magnetic focusing

Let us now turn to the issue of magnetic focusing under the influence of spin-orbit coupling. A magnetic focusing experiment is conceptually very simple and sketched in Fig. 6: Electrons enter a quantum well at a location $x = x_i$, follow a ballistic cyclotron orbit, and impinge again on the boundary of the system at a location $x = x_f$. In the absence of spin-orbit coupling, this difference in coordinate depends, just as in the classical case, only on the applied magnetic field and the initial group wave number k_0 , $x_f - x_i = 2k_0 \ell^2$. Thus, using an appropriately located detection contact one can study electron transport as a function of these two quantities.

In a typical experiment, however, rather the energy E of electrons (defined by the Fermi energy of the injecting lead) not their momentum is fixed with both quantities being connected via Eq. (17). Therefore, the wave number k_0 of an injected electron will in general depend on its spin state; only in the absence of both Zeeman coupling and spin-orbit interaction k_0 is independent of the electron spin. In turn, for random initial spin directions, $x_f - x_i$ will be distributed according to some probability density $P_x(x_f - x_i)$. Fig. 7 shows a numerical evaluation of $P_x(x_f - x_i)$ for a wave packet of width $d = \ell$, total and energy $E = 2.0\hbar\omega$ at zero Zeeman coupling and different Rashba energies. The initial angular coordinates $\cos\theta$ and φ determining the complex amplitudes κ and λ in the initial state (14) were chosen at random from uniform distributions in the interval $[-1, 1]$ and $[0, 2\pi]$, respectively. The data is averaged over 500000 randomly chosen initial spin states each. At a small Rashba energy of only $\varepsilon_R = m(\alpha/\hbar)^2 = 0.01\hbar\omega$ (top left panel) the dynamics depend only very weakly on spin and $P_x(x_f - x_i)$ is strongly peaked around $x_f - x_i = 2k_0 \ell^2 \approx 3.16$, the classical cyclotron diameter expected in the absence of spin-orbit coupling. With increasing Rashba energy, this peak undergoes a broadening with the maximum of the probability density being located at smaller values of $x_f - x_i$. Fig. 8 shows the same type of data at a Zeeman energy of $\varepsilon_Z = 0.1\hbar\omega$ which does not lead to any qualitative difference.

In summary, the initial narrow peak of the probability density $P_x(x_f - x_i)$ at small spin-orbit coupling broadens with increasing Rashba energy and develops a non-trivial structure in terms of a maximum at small arguments with a broad shoulder reaching to higher values. The structures seen in Figs. 7, 8 appear to be somewhat

different to the results of Ref.¹¹ where a splitting of the conductance peak as a function of magnetic field was found for increasing Rashba coupling. These two peaks can be related to two different effective cyclotron radii corresponding to two initial spin states with respect to a quantization axis being perpendicular to the initial momentum and the magnetic field, an observation similar to the “strong coupling” semiclassical scenario of Ref.²⁷. Thus, in the light of these investigations one could also expect a double-peak structure to develop in the probability density $P_x(x_f - x_i)$. However, the investigations of Ref.¹¹ work at clearly higher electron energies compared to the cyclotron energy, and Landau quantization is explicitly neglected. This is in contrast to the present study which works at larger cyclotron energies taking into account the full quantum dynamics of the problem.

IV. CONCLUSIONS AND OUTLOOK

We have studied the ballistic motion of electrons in III-V semiconductor quantum wells with Rashba spin-orbit coupling and a perpendicular magnetic field. Differently from previous investigations, our numerical approach takes into account the full quantum mechanics of the problem and is technically limited to situations where the cyclotron energy is of the same order as the energy of the initial electron wave packet. For typical experimental parameters, this restriction corresponds to magnetic fields of a few tesla. Such fields are larger than those considered previously in circumstances of semiclassical neglecting Landau quantization, and in this sense our present study is complementary to such semiclassical approaches. As a result, in the parameter regime considered here the electron dynamics are particularly rich and not adequately described by semiclassical approximations. An interesting issue for further investigations here includes the question whether the seemingly “chaotic” trajectories shown in section III A are truly ergodic. Moreover, it is tempting to attribute the irregularity of these trajectories to the *zitterbewegung* predicted previously for electron motion in two-dimensional electron gases without magnetic fields^{16,17,18,19,20,21,22,23,24,25,26,27,28}. What both phenomena have indeed in common is the fact that they are the result of spin-orbit coupling, and the irregular motion of electrons in a perpendicular magnetic field is the consequence of the non-equidistant spectrum of Landau levels induced by spin-orbit interaction.

In this study, we have concentrated on spin-orbit coupling of the Rashba type. However, the situation of linear Dresselhaus coupling can be treated analogously³¹ as it only couples, like the Rashba term, pairs of neighboring Landau levels with opposite spin. If both types of spin-orbit coupling terms are present, all Landau levels are coupled, and the single-particle Hamiltonian cannot be diagonalized analytically anymore. In this case the eigensystem of the Hamiltonian needs to be computed numerically, or appropriate approximations have to be

employed¹³. It is an interesting question whether the inclusion of both kinds of couplings leads to qualitatively new observations. A particular situation is reached if both terms occur with the same magnitude, where, for zero Zeeman coupling, a new conserved spin operator arises³⁶.

Further possible extensions of the present work include the study of valence-band holes (as opposed to conduction-band electrons) with an effective spin-orbit coupling being trilinear in the momentum, and electron or hole dynamics under the influence of an additional in-plane electric field.

Acknowledgments

I thank S. Q. Shen and U. Zülicke for useful discussions. This work was supported by DFG via SFB 689 “Spin Phenomena in reduced Dimensions”.

APPENDIX A: TECHNICAL DETAILS

1. Overlap with basis states

The overlap of the initial orbital state (15) and the basis states (13) of the usual Landau levels can be expressed as

$$\begin{aligned} \langle n, k | \phi \rangle &= (-i)^n \sqrt{\frac{2}{n!2^n}} \sqrt{\frac{d}{\pi}} \frac{\sqrt{\frac{d}{\ell}}}{\sqrt{1 + \frac{d^2}{\ell^2}}} \left(\frac{1 - \frac{d^2}{\ell^2}}{1 + \frac{d^2}{\ell^2}} \right)^{n/2} \\ &\times \exp \left(-\frac{1}{2} \frac{k_0^2 \ell^2}{1 + \frac{d^2}{\ell^2}} - \frac{d^2}{2} (k - k_0)^2 \right) \\ &\times H_n \left(-\frac{k_0 \ell}{\sqrt{(1 - \frac{d^2}{\ell^2})(1 + \frac{d^2}{\ell^2})}} \right) \end{aligned} \quad (A1)$$

$$\begin{aligned} &= (-i)^n \sqrt{\frac{2}{n!2^n}} \sqrt{\frac{d}{\pi}} \frac{\sqrt{\frac{d}{\ell}}}{\sqrt{1 + \frac{d^2}{\ell^2}}} \\ &\times \exp \left(-\frac{1}{2} \frac{k_0^2 \ell^2}{1 + \frac{d^2}{\ell^2}} - \frac{d^2}{2} (k - k_0)^2 \right) \\ &\times \sum_{p=0}^{\lfloor \frac{n}{2} \rfloor} \left[\frac{(-1)^p}{p!} \frac{n!}{(n-2p)!} (-2k_0 \ell)^{n-2p} \right. \\ &\quad \left. \left(1 - \frac{d^2}{\ell^2} \right)^p \left(1 + \frac{d^2}{\ell^2} \right)^{p-n} \right], \end{aligned} \quad (A2)$$

where $\lfloor x \rfloor$ denotes the largest integer not larger than x , and the second of the above equations shows explicitly that the overlap is well-behaved at $d = \ell$. The above expressions can be obtained by using the explicit form of

the Hermite polynomials,

$$H_n(x) = (-1)^n e^{x^2} \frac{d^n}{dx^n} e^{-x^2} \quad (\text{A3})$$

$$= \sum_{p=0}^{\lfloor \frac{n}{2} \rfloor} \left[\frac{(-1)^p}{p!} \frac{n!}{(n-2p)!} (2x)^{n-2p} \right]. \quad (\text{A4})$$

Finally, the overlap of the initial state (14) with the spinful eigenstates (4) is given by

$$\langle 0, k, \uparrow | \psi \rangle = \kappa \langle 0, k | \phi \rangle, \quad (\text{A5})$$

$$\langle n, k, \mu | \psi \rangle = \bar{u}_n^\mu \kappa \langle n, k | \phi \rangle + \bar{v}_n^\mu \lambda \langle n-1, k | \phi \rangle. \quad (\text{A6})$$

2. Matrix elements

As already stated, the matrix elements of the kinetic momentum as well as the spin operators are diagonal with respect to the wave number k . For the kinetic momentum, the matrix elements read explicitly

$$\langle 0, k, \uparrow | \pi_x | n, k, \mu \rangle = \frac{\hbar}{\ell\sqrt{2}} u_1^\mu \delta_{1,n}, \quad (\text{A7})$$

$$\langle 0, k, \uparrow | \pi_y | n, k, \mu \rangle = \frac{-i\hbar}{\ell\sqrt{2}} u_1^\mu \delta_{1,n}, \quad (\text{A8})$$

$$\begin{aligned} & \langle n_1, k, \mu_1 | \pi_x | n_2, k, \mu_2 \rangle \\ &= (\sqrt{n_1+1} \bar{u}_{n_1+1}^{\mu_1} u_{n_1+1}^{\mu_2} + \sqrt{n_1} \bar{v}_{n_1}^{\mu_1} v_{n_1+1}^{\mu_2}) \\ & \quad \times \frac{\hbar}{\ell\sqrt{2}} \delta_{n_1, n_2-1} \\ &+ (\sqrt{n_1} \bar{u}_{n_1}^{\mu_1} u_{n_1-1}^{\mu_2} + \sqrt{n_1-1} \bar{v}_{n_1}^{\mu_1} v_{n_1-1}^{\mu_2}) \\ & \quad \times \frac{\hbar}{\ell\sqrt{2}} \delta_{n_1, n_2+1}, \quad (\text{A9}) \\ & \langle n_1, k, \mu_1 | \pi_y | n_2, k, \mu_2 \rangle \\ &= (\sqrt{n_1+1} \bar{u}_{n_1+1}^{\mu_1} u_{n_1+1}^{\mu_2} + \sqrt{n_1} \bar{v}_{n_1}^{\mu_1} v_{n_1+1}^{\mu_2}) \\ & \quad \times \frac{-i\hbar}{\ell\sqrt{2}} \delta_{n_1, n_2-1} \\ &+ (\sqrt{n_1} \bar{u}_{n_1}^{\mu_1} u_{n_1-1}^{\mu_2} + \sqrt{n_1-1} \bar{v}_{n_1}^{\mu_1} v_{n_1-1}^{\mu_2}) \\ & \quad \times \frac{i\hbar}{\ell\sqrt{2}} \delta_{n_1, n_2+1}. \quad (\text{A10}) \end{aligned}$$

The in-plane components of the spin operator have the matrix elements

$$\langle 0, k, \uparrow | \sigma^x | n, k, \mu \rangle = v_1^\mu \delta_{1,n}, \quad (\text{A11})$$

$$\langle 0, k, \uparrow | \sigma^y | n, k, \mu \rangle = -iv_1^\mu \delta_{1,n}, \quad (\text{A12})$$

$$\begin{aligned} \langle n_1, k, \mu_1 | \sigma^x | n_2, k, \mu_2 \rangle &= \bar{u}_{n_1}^{\mu_1} v_{n_1+1}^{\mu_2} \delta_{n_1, n_2-1} \\ &+ \bar{v}_{n_1}^{\mu_1} u_{n_1+1}^{\mu_2} \delta_{n_1, n_2+1}, \quad (\text{A13}) \end{aligned}$$

$$\begin{aligned} \langle n_1, k, \mu_1 | \sigma^y | n_2, k, \mu_2 \rangle &= -i \bar{u}_{n_1}^{\mu_1} v_{n_1+1}^{\mu_2} \delta_{n_1, n_2-1} \\ &- i \bar{v}_{n_1}^{\mu_1} u_{n_1+1}^{\mu_2} \delta_{n_1, n_2+1}, \quad (\text{A14}) \end{aligned}$$

whereas σ^z is diagonal in the Landau level index n , and the nonvanishing matrix elements read

$$\langle 0, k, \uparrow | \sigma^z | 0, k, \uparrow \rangle = 1, \quad (\text{A15})$$

$$\langle n, k, \mu_1 | \sigma^z | n, k, \mu_2 \rangle = \bar{u}_n^{\mu_1} u_n^{\mu_2} - \bar{v}_n^{\mu_1} v_n^{\mu_2}. \quad (\text{A16})$$

3. Explicit time evolution

Using the expressions given in the previous sections, the time-evolved expectation values of the components of the kinetic momentum can be formulated as

$$\begin{aligned}
\langle (\pi_x)_H(t) \rangle &= \text{Re} \left\{ \sqrt{2} \frac{\hbar}{\ell} \sum_{\mu=\pm} e^{\frac{i}{\hbar}(\varepsilon_0 - \varepsilon_1^\mu)t} (|\kappa|^2 |u_1^\mu|^2 J_0 + \bar{\kappa} \lambda u_1^\mu \bar{v}_1^\mu I_0) \right\} \\
&+ \text{Re} \left\{ \sqrt{2} \frac{\hbar}{\ell} \sum_{n=1}^{\infty} \sum_{\mu_1, \mu_2=\pm} e^{\frac{i}{\hbar}(\varepsilon_n^{\mu_1} - \varepsilon_{n+1}^{\mu_2})t} \left[|\kappa|^2 (\sqrt{n+1} |u_n^{\mu_1}|^2 |u_{n+1}^{\mu_2}|^2 + \sqrt{n} u_n^{\mu_1} \bar{v}_n^{\mu_1} \bar{u}_{n+1}^{\mu_2} v_{n+1}^{\mu_2}) J_n \right. \right. \\
&\quad + |\lambda|^2 (\sqrt{n+1} \bar{u}_n^{\mu_1} v_n^{\mu_1} u_{n+1}^{\mu_2} \bar{v}_{n+1}^{\mu_2} + \sqrt{n} |v_n^{\mu_1}|^2 |v_{n+1}^{\mu_2}|^2) J_{n-1} \\
&\quad + \bar{\kappa} \lambda (\sqrt{n+1} |u_n^{\mu_1}|^2 u_{n+1}^{\mu_2} \bar{v}_{n+1}^{\mu_2} + \sqrt{n} u_n^{\mu_1} \bar{v}_n^{\mu_1} |v_{n+1}^{\mu_2}|^2) I_n \\
&\quad \left. \left. + \kappa \bar{\lambda} (\sqrt{n+1} \bar{u}_n^{\mu_1} v_n^{\mu_1} |u_{n+1}^{\mu_2}|^2 + \sqrt{n} |v_n^{\mu_1}|^2 \bar{u}_{n+1}^{\mu_2} v_{n+1}^{\mu_2}) K_n \right] \right\}, \quad (\text{A17})
\end{aligned}$$

$$\begin{aligned}
\langle (\pi_y)_H(t) \rangle &= \text{Re} \left\{ -i \sqrt{2} \frac{\hbar}{\ell} \sum_{\mu=\pm} e^{\frac{i}{\hbar}(\varepsilon_0 - \varepsilon_1^\mu)t} (|\kappa|^2 |u_1^\mu|^2 J_0 + \bar{\kappa} \lambda u_1^\mu \bar{v}_1^\mu I_0) \right\} \\
&+ \text{Re} \left\{ -i \sqrt{2} \frac{\hbar}{\ell} \sum_{n=1}^{\infty} \sum_{\mu_1, \mu_2=\pm} e^{\frac{i}{\hbar}(\varepsilon_n^{\mu_1} - \varepsilon_{n+1}^{\mu_2})t} \left[|\kappa|^2 (\sqrt{n+1} |u_n^{\mu_1}|^2 |u_{n+1}^{\mu_2}|^2 + \sqrt{n} u_n^{\mu_1} \bar{v}_n^{\mu_1} \bar{u}_{n+1}^{\mu_2} v_{n+1}^{\mu_2}) J_n \right. \right. \\
&\quad + |\lambda|^2 (\sqrt{n+1} \bar{u}_n^{\mu_1} v_n^{\mu_1} u_{n+1}^{\mu_2} \bar{v}_{n+1}^{\mu_2} + \sqrt{n} |v_n^{\mu_1}|^2 |v_{n+1}^{\mu_2}|^2) J_{n-1} \\
&\quad + \bar{\kappa} \lambda (\sqrt{n+1} |u_n^{\mu_1}|^2 u_{n+1}^{\mu_2} \bar{v}_{n+1}^{\mu_2} + \sqrt{n} u_n^{\mu_1} \bar{v}_n^{\mu_1} |v_{n+1}^{\mu_2}|^2) I_n \\
&\quad \left. \left. + \kappa \bar{\lambda} (\sqrt{n+1} \bar{u}_n^{\mu_1} v_n^{\mu_1} |u_{n+1}^{\mu_2}|^2 + \sqrt{n} |v_n^{\mu_1}|^2 \bar{u}_{n+1}^{\mu_2} v_{n+1}^{\mu_2}) K_n \right] \right\}, \quad (\text{A18})
\end{aligned}$$

where we have defined

$$I_n = \int_{-\infty}^{\infty} dk \langle \phi | n, k \rangle \langle n, k | \phi \rangle, \quad (\text{A19})$$

$$J_n = \int_{-\infty}^{\infty} dk \langle \phi | n, k \rangle \langle n+1, k | \phi \rangle, \quad (\text{A20})$$

$$K_n = \int_{-\infty}^{\infty} dk \langle \phi | n-1, k \rangle \langle n+1, k | \phi \rangle. \quad (\text{A21})$$

Using Eq. (A2) it is straightforward to derive explicit expressions for these integrals in terms of finite sums to be evaluated numerically. As an example, for I_n one finds

$$I_n = \frac{\frac{d^2}{\ell^2}}{1 + \frac{d^2}{\ell^2}} \sum_{p,q=0}^{\left[\frac{n}{2}\right]} \left[\frac{(-1)^{p+q}}{p!q!} \frac{n! 2^{n+1-2(p+q)}}{(n-2p)!(n-2q)!} \left(1 - \frac{d^2}{\ell^2}\right)^{p+q} \left(\frac{1}{1 + \frac{d^2}{\ell^2}}\right)^{2n-(p+q)} R_{n-(p+q)}(\ell, d, k_0) \right] \quad (\text{A22})$$

with

$$\begin{aligned}
R_m(\ell, d, k_0) &= \frac{\ell}{\sqrt{\pi}} \int_{-\infty}^{\infty} dk (k\ell)^{2m} \exp \left(- \left(\frac{(k\ell)^2}{1 + \frac{d^2}{\ell^2}} + d^2(k - k_0)^2 \right) \right) \\
&= \left(\frac{\ell^4 + d^2 \ell^2}{\ell^4 + d^2 \ell^2 + d^4} \right)^{m+1/2} \exp \left(- \frac{\ell^4 d^2 k_0^2}{\ell^4 + d^2 \ell^2 + d^4} \right) \left(-\frac{1}{4} \right)^m H_{2m} \left(i \sqrt{\frac{\ell^4 + d^2}{\ell^4 + d^2 \ell^2 + d^4}} d^2 k_0 \right). \quad (\text{A23})
\end{aligned}$$

Note that, despite the imaginary argument of the Hermite polynomial H_{2m} , R_m is always real and positive.

Thus computing the quantities I_n (and similarly J_n and

K_n) requires again the evaluation of Hermite polynomials. At large Landau level index n this operation limits the accuracy of the present numerical approach. Given the data I_n , J_n , K_n , the summations (A17), (A18) are to be performed numerically where the sum over the Landau level index n can be truncated at a sufficiently large energy. For the simulations presented in this work it is sufficient to take into account the first 25 Landau levels where the evaluation of Hermite polynomials is numerically unproblematic.

It is noteworthy that the quantities I_n , J_n , K_n fulfill certain sum rules which provide a convenient check on numerical evaluations. For instance, normalization of the initial state $|\phi\rangle$ obviously requires

$$\sum_{n=0}^{\infty} I_n = 1. \quad (\text{A24})$$

Moreover, we have

$$\begin{aligned} \sum_{n=0}^{\infty} \sqrt{n+1} J_n &= \langle \phi | a | \phi \rangle \\ &= \frac{i}{\sqrt{2}} k_0 \ell. \end{aligned} \quad (\text{A25})$$

Analogously one derives

$$\sum_{n=0}^{\infty} \sqrt{n(n+1)} K_n = -\frac{1}{4} \frac{d^2}{\ell^2} - \frac{1}{2} k_0^2 \ell^2. \quad (\text{A26})$$

Finally, coming back to physical expectation values, the time-evolved spin components read

$$\begin{aligned} \langle (\sigma_H^x(t)) \rangle &= \text{Re} \left\{ 2 \sum_{\mu=\pm} e^{\frac{i}{\hbar}(\varepsilon_0 - \varepsilon_1^\mu)t} (|\kappa|^2 \bar{u}_1^\mu v_1^\mu J_0 + \bar{\kappa} \lambda |v_1^\mu|^2 I_0) \right\} \\ &+ \text{Re} \left\{ 2 \sum_{n=1}^{\infty} \sum_{\mu_1, \mu_2=\pm} e^{\frac{i}{\hbar}(\varepsilon_n^{\mu_1} - \varepsilon_{n+1}^{\mu_2})t} \left[|\kappa|^2 |u_n^{\mu_1}|^2 \bar{u}_{n+1}^{\mu_2} v_{n+1}^{\mu_2} J_n + |\lambda|^2 \bar{u}_n^{\mu_1} v_n^{\mu_1} |v_{n+1}^{\mu_2}|^2 J_{n-1} \right. \right. \\ &\quad \left. \left. + \bar{\kappa} \lambda |u_n^{\mu_1}|^2 |v_{n+1}^{\mu_2}|^2 I_n + \kappa \bar{\lambda} \bar{u}_n^{\mu_1} v_n^{\mu_1} \bar{u}_{n+1}^{\mu_2} v_{n+1}^{\mu_2} K_n \right] \right\}, \end{aligned} \quad (\text{A27})$$

$$\begin{aligned} \langle (\sigma_H^y(t)) \rangle &= \text{Re} \left\{ -2i \sum_{\mu=\pm} e^{\frac{i}{\hbar}(\varepsilon_0 - \varepsilon_1^\mu)t} (|\kappa|^2 \bar{u}_1^\mu v_1^\mu J_0 + \bar{\kappa} \lambda |v_1^\mu|^2 I_0) \right\} \\ &+ \text{Re} \left\{ -2i \sum_{n=1}^{\infty} \sum_{\mu_1, \mu_2=\pm} e^{\frac{i}{\hbar}(\varepsilon_n^{\mu_1} - \varepsilon_{n+1}^{\mu_2})t} \left[|\kappa|^2 |u_n^{\mu_1}|^2 \bar{u}_{n+1}^{\mu_2} v_{n+1}^{\mu_2} J_n + |\lambda|^2 \bar{u}_n^{\mu_1} v_n^{\mu_1} |v_{n+1}^{\mu_2}|^2 J_{n-1} \right. \right. \\ &\quad \left. \left. + \bar{\kappa} \lambda |u_n^{\mu_1}|^2 |v_{n+1}^{\mu_2}|^2 I_n + \kappa \bar{\lambda} \bar{u}_n^{\mu_1} v_n^{\mu_1} \bar{u}_{n+1}^{\mu_2} v_{n+1}^{\mu_2} K_n \right] \right\}, \end{aligned} \quad (\text{A28})$$

$$\begin{aligned} \langle (\sigma_H^z(t)) \rangle &= |\kappa|^2 I_0 + \sum_{n=1}^{\infty} \sum_{\mu_1, \mu_2=\pm} e^{\frac{i}{\hbar}(\varepsilon_n^{\mu_1} - \varepsilon_{n+1}^{\mu_2})t} \left[|\kappa|^2 u_n^{\mu_1} (\bar{u}_n^{\mu_1} u_n^{\mu_2} - \bar{v}_n^{\mu_1} v_n^{\mu_2}) \bar{u}_n^{\mu_2} I_n \right. \\ &\quad + |\lambda|^2 v_n^{\mu_1} (\bar{u}_n^{\mu_1} u_n^{\mu_2} - \bar{v}_n^{\mu_1} v_n^{\mu_2}) \bar{v}_n^{\mu_2} I_{n-1} \\ &\quad + \bar{\kappa} \lambda u_n^{\mu_1} (\bar{u}_n^{\mu_1} u_n^{\mu_2} - \bar{v}_n^{\mu_1} v_n^{\mu_2}) \bar{v}_n^{\mu_2} J_{n-1} \\ &\quad \left. + \kappa \bar{\lambda} v_n^{\mu_1} (\bar{u}_n^{\mu_1} u_n^{\mu_2} - \bar{v}_n^{\mu_1} v_n^{\mu_2}) \bar{u}_n^{\mu_2} J_{n-1} \right]. \end{aligned} \quad (\text{A29})$$

¹ S. Datta and B. Das, Appl. Phys. Lett. **56**, 665 (1990).

² H. van Houten, C. W. J. Beenakker, J. G. Williamson, M. E. I. Broekaart, P. H. M. van Loosdrecht, B. J. van Wees, J. E. Mooij, C. T. Foxon, and J. J. Harris, Phys. Rev. B **39**, 8556 (1989).

³ J. J. Heremans, M. B. Santos, and M. Shayegan, Appl.

Phys. Lett. **61**, 1652 (1992).

⁴ J. J. Heremans, M. B. Santos, and M. Shayegan, Surf. Sci. **305**, 348 (1993).

⁵ K.E. Aidala, R.E. Parrott, T. Kramer, E. J. Heller, R. M. Westervelt, M. P. Hanson, and A. C. Gossard, Nature Phys. **3**, 464 (2007).

- ⁶ R. M. Potok, J. A. Folk, C. M. Marcus, and V. Umansky, Phys. Rev. Lett. **89**, 266602 (2002).
- ⁷ L. P. Rokhinson, V. Larkina, Y. B. Lyanda-Geller, L. N. Pfeiffer, and K. W. West, Phys. Rev. Lett. **93**, 146601 (2004).
- ⁸ L. P. Rokhinson, L. N. Pfeiffer, and K. W. West, Phys. Rev. Lett. **96**, 156602 (2006).
- ⁹ A. R. Dedigama, D. Deen, S. Q. Murphy, N. Goel, J. C. Keay, K. Suzuki, S. Miyashita, and Y. Hirayama, Physica E **34**, 647 (2006).
- ¹⁰ G. Goldoni and A. Fasolino, Phys. Rev. B **44**, 8369 (1991).
- ¹¹ G. Usaj and C. A. Balseiro, Phys. Rev. B **70**, 041301 (2004).
- ¹² A. Reynoso, G. Usaj, M. J. Sanchez, and C. A. Balseiro, Phys. Rev. B **70**, 235344 (2004).
- ¹³ M. Valin-Rodriguez and R. G. Nazmitdinov, Phys. Rev. B **73**, 235306 (2006).
- ¹⁴ A. Reynoso, G. Usaj, and C. A. Balseiro, Phys. Rev. B **75**, 085321 (2007).
- ¹⁵ A. Reynoso, G. Usaj, and C. A. Balseiro, arXiv:cond-mat/0703267.
- ¹⁶ J. Schliemann, D. Loss, and R. M. Westervelt, Phys. Rev. Lett. **94**, 206801 (2005).
- ¹⁷ J. Schliemann, D. Loss, and R. M. Westervelt, Phys. Rev. B **73**, 085323 (2006).
- ¹⁸ W. Zawadzki, Phys. Rev. B **72**, 085217 (2005); Phys. Rev. B **74**, 205439 (2006).
- ¹⁹ B. K. Nikolic, L. P. Zarbo, and S. Welack, Phys. Rev. B **72**, 075335 (2005).
- ²⁰ S.-Q. Shen, Phys. Rev. Lett. **95**, 187203 (2005).
- ²¹ J. Cserti and G. David, Phys. Rev. B **74**, 172305 (2006).
- ²² P. Brushein and H. Q. Xu, Phys. Rev. B **74**, 205307 (2006).
- ²³ T. M. Rusin and W. Zawadzki, J. Phys.: Condens. Mat. **19**, 136219 (2007).
- ²⁴ J. Schliemann, Phys. Rev. B **75**, 045304 (2007).
- ²⁵ R. Winkler, U. Zülicke, and J. Bolte, Phys. Rev. B **75**, 205314 (2007).
- ²⁶ E. Bernardes, J. Schliemann, M. Lee, J. C. Egues, and D. Loss, Phys. Rev. Lett. **99**, 076603 (2007).
- ²⁷ U. Zülicke, J. Bolte, and R. Winkler, New J. Phys. **9**, 355 (2007).
- ²⁸ U. Zülicke, J. Bolte, and R. Winkler, arXiv:0707.3701.
- ²⁹ E. Schrödinger, Sitzungsber. Preuss. Akad. Wiss. Phys. Math. Klass. **24**, 418 (1930).
- ³⁰ E. I. Rashba, Fiz. Tverd. Tela (Leningrad) **2**, 1224 (1960) (Sov. Phys. Solid State **2**, 1109 (1960)); Y. A. Bychkov and E. I. Rashba, J. Phys. C **17**, 6039 (1984).
- ³¹ J. Schliemann, J. C. Egues, and D. Loss, Phys. Rev. B **67**, 085302 (2003).
- ³² J. R. Ackerhalt and K. Rzazewski, Phys. Rev. A **12**, 2549 (1975).
- ³³ S. M. Barnett and P. M. Radmore, *Methods in Theoretical Quantum Optics*, Clarendon Press, Oxford 1997.
- ³⁴ J. Schliemann, A. V. Khaetskii, and Daniel Loss, Phys. Rev. B **66**, 245303 (2002).
- ³⁵ C. H. Bennett, H. J. Bernstein, S. Popescu, and B. Schumacher, Phys. Rev. A **53**, 2046 (1996).
- ³⁶ J. Schliemann, J. C. Egues, and D. Loss, Phys. Rev. Lett. **90**, 146801 (2003).

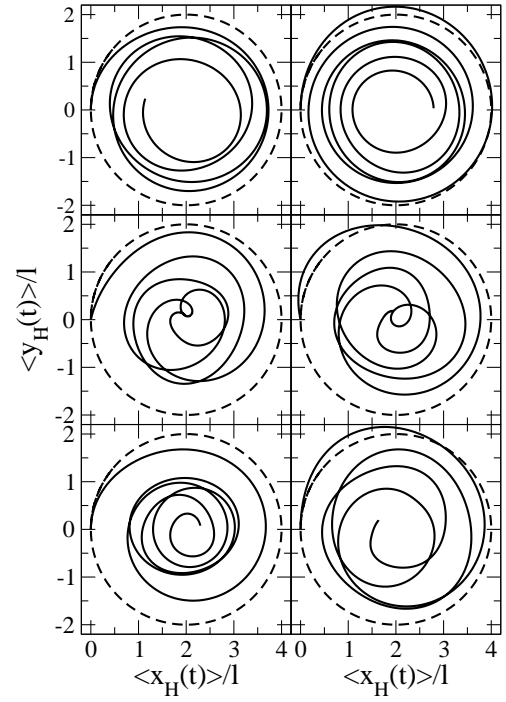


FIG. 1: Orbital dynamics of a wave packet of initial width $d = 1.0\ell$ and group wave number $k_0 = 2.0/\ell$ for various initial spin states. The Rashba energy is $\varepsilon_R = 0.2\hbar\omega_c$ while the Zeeman energy is put to zero. In the left (right) top panel, the spin points initially along the positive (negative) x -direction. The middle and bottom panels show the corresponding data for the y - and z -direction, respectively. The simulation time is always $t = 30/\omega_c$. The strictly circular motion (dotted lines) with radius $k_0\ell^2$ occurring in the absence of spin-orbit coupling is always shown as a guide to the eye.

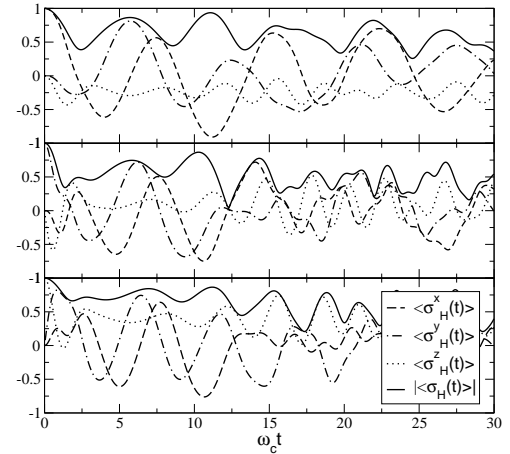


FIG. 2: Spin dynamics as expressed in terms of the time-dependent expectation values corresponding to the left column of Fig. 1. The solid lines show the quantity $|\langle \vec{\sigma}_H(t) \rangle|$ which is a measure of entanglement between the spin and the orbital degrees of freedom.

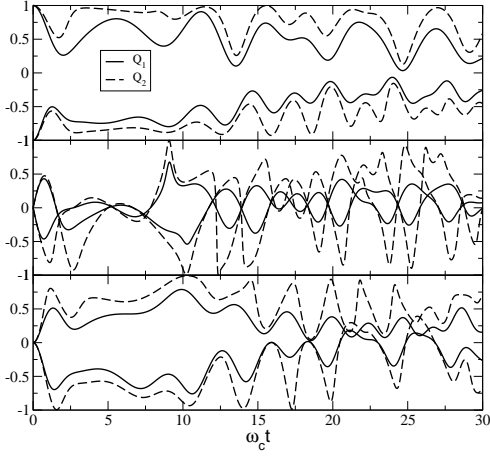


FIG. 3: The quantities Q_1 (solid lines) and Q_2 (dashed lines) defined in the text as a function of time for the same system parameters as in Fig. 1. In the top panel, the spin points initially along the positive (negative) x -direction with $Q_1(0) = Q_2(0) = +1$ ($Q_1(0) = Q_2(0) = -1$). The middle and bottom panel show the analogous data with the spin initially aligned along the y - and z -axis, respectively. Here we have always $Q_1(0) = Q_2(0) = 0$.

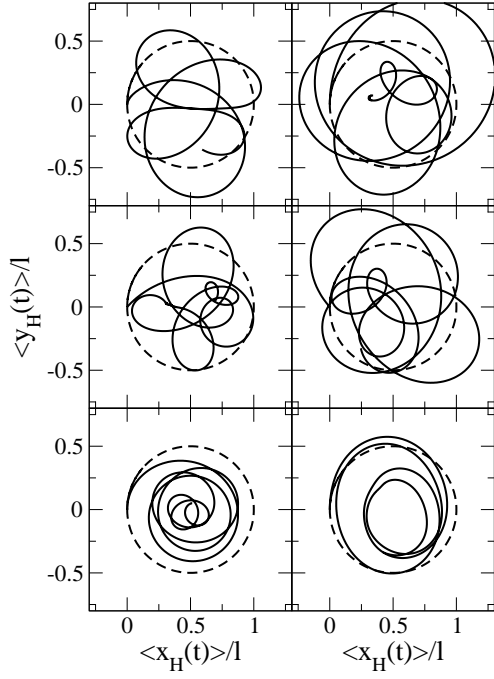


FIG. 4: Orbital dynamics for the same system as in Fig. 1 but with a smaller initial group wave number of only $k_0 = 0.5/\ell$. Again, the strictly circular motion occurring in the absence of spin-orbit coupling is always shown as a guide to the eye.

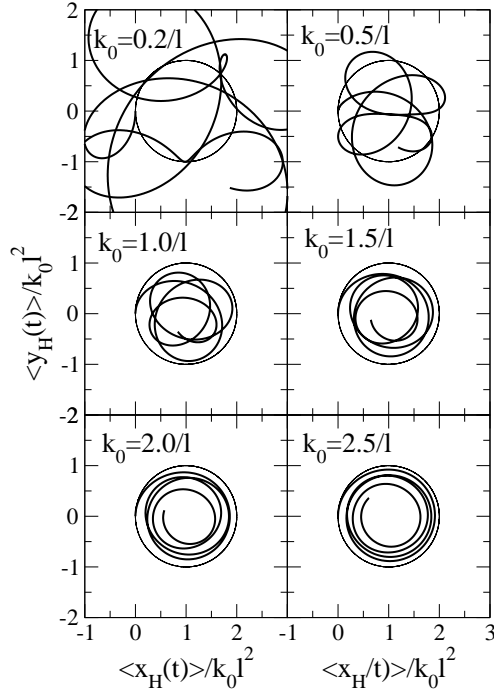


FIG. 5: Orbital dynamics for the same system as in Fig. 1 for various values of the initial group wave number k_0 and the spin initially always pointing along the positive x -axis. For a better comparison the components of $\langle \vec{r} \rangle$ are given in units of $k_0 \ell^2$.

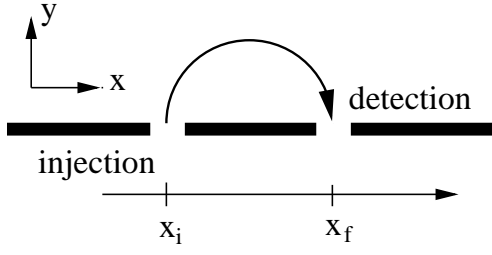


FIG. 6: Schematic sketch of a magnetic focusing experiment.

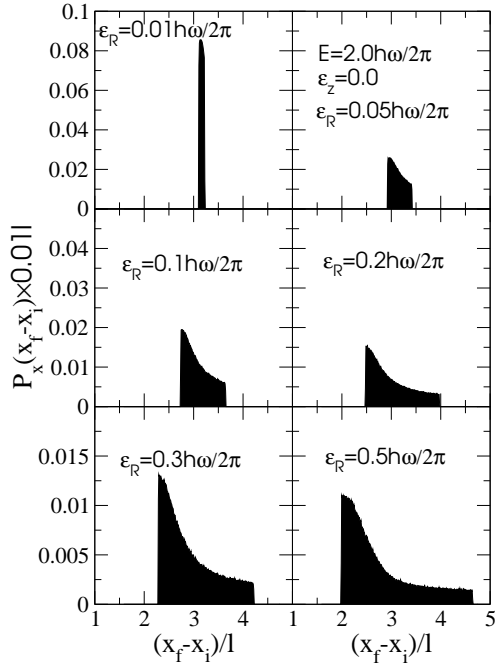


FIG. 7: The probability density $P_x(x_f - x_i)$ for a wave packet of width $d = \ell$, total and energy $E = 2.0\hbar\omega$ at zero Zeeman coupling and different Rashba energies. The data is averaged over 500000 randomly chosen initial spin states each. Note the different scale of the y -axis in the top, middle, and bottom panels.

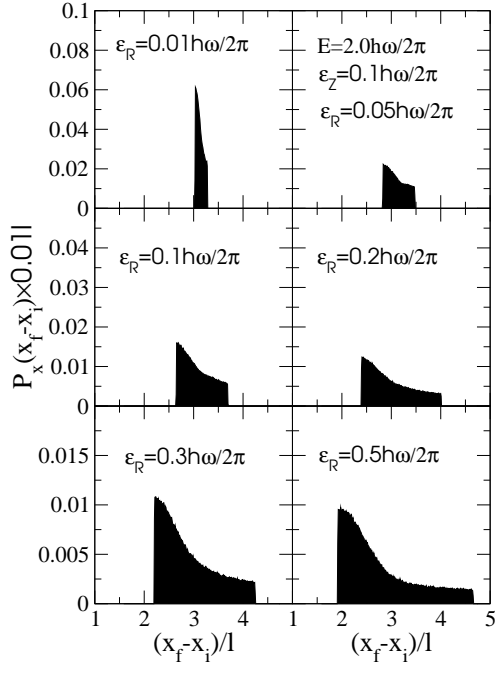


FIG. 8: The probability density $P_x(x_f - x_i)$ for the same situation as in Fig.7 but with a Zeeman energy of $\epsilon_z = 0.1 \hbar \omega$.